Solar Phys (2008) 253: 305–317
DOI 10.1007/s11207-008-9220-x



# A Flare-Generated Shock during a Coronal Mass Ejection on 24 December 1996

**J. Magdalenić · B. Vršnak · S. Pohjolainen · M. Temmer · H. Aurass · N.J. Lehtinen**

Received: 25 January 2008 / Accepted: 31 May 2008 / Published online: 16 July 2008


**Abstract** We present a multiwavelength study of the large-scale coronal disturbances associated with the CME – flare event recorded on 24 December 1996. The kinematics of the shock wave signature, the type II radio burst, is analyzed and compared with the flare evolution and the CME kinematics. We employ radio dynamic spectra, position of the Nançay Radioheliograph sources, and LASCO-C1 observations, providing detailed study of this limb event. The obtained velocity of the shock wave is significantly higher than the contemporaneous CME velocity (1000 and 235 km $s^{-1}$, respectively). Moreover, since the main acceleration phase of the CME took place 10 – 20 min after the shock wave was launched, we

Radio Physics and the Flare-CME Relationship
Guest Editors: Karl-Ludwig Klein and Silja Pohjolainen

J. Magdalenić is now also at SIDC, Royal Observatory of Belgium, Av. Circulaire 3, 1180 Brussels, Belgium.

J. Magdalenić (✉) · B. Vršnak · M. Temmer
Hvar Observatory, Faculty of Geodesy, Kačićeva 26, 10000 Zagreb, Croatia
e-mail: mjasmina@geof.hr

B. Vršnak
e-mail: bvrsnak@geof.hr

S. Pohjolainen · N.J. Lehtinen
Tuorla Observatory, University of Turku, Turku, Finland

S. Pohjolainen
e-mail: silpoh@utu.fi

N.J. Lehtinen
e-mail: nijole@utu.fi

M. Temmer
Space Research Institute, Austrian Academy of Sciences, Schmiedlstrasse 6, 8042 Graz, Austria
e-mail: manuela.temmer@uni-graz.at

H. Aurass
Astrophysical Institute Potsdam, 14482 Potsdam, Germany
e-mail: haurass@aip.de

conclude that the shock wave on 24 December 1996 was probably not driven by the CME. However, the shock wave was closely associated with the flare impulsive phase, indicating that it was ignited by the energy release in the flare.

**Keywords** Flares, waves · Coronal mass ejections, initiation and propagation · Radio bursts, type II · Waves, shock

## 1. Introduction

Coronal large-amplitude MHD disturbances associated with type II radio bursts (Nelson and Melrose, 1985) and chromospheric Moreton waves (Moreton and Ramsey, 1960) are closely linked to coronal mass ejections (CMEs) and flares. In the sweeping-skirt hypothesis by Uchida (1968, 1974), the Moreton wave is considered as a surface signature of the coronal fast-mode MHD shock that excites a type II burst higher up in the corona. Widely studied type II radio bursts are attributed to the shock-accelerated electrons that excite plasma waves, which are converted into escaping radio waves (McLean and Labrum, 1985).

In a longstanding debate coronal shock waves have been attributed either to solar flares or CMEs or to some combination of these phenomena (see Cliver, Webb, and Howard, 1999; Vršnak *et al.*, 2001, and references therein). Since CMEs and flares are usually very closely synchronized it is difficult to make a decisive conclusion.

Certainly, CMEs play a very important role in formation of the coronal waves (Biesecker *et al.*, 2002), and most of the interplanetary shocks are driven by CMEs (Reiner *et al.*, 2001; Oh, Yi, and Kim, 2007). However, it remains unclear whether coronal shocks are CME driven (Cliver *et al.*, 2004) or flare ignited (Vršnak, 2001). Some aspects of the wave–flare/CME relationship, such as timing, spatial relationship, wavefront shape, *etc.*, in some detailed case studies strongly favor the flare-ignited scenario (Hudson *et al.*, 2003; Warmuth *et al.*, 2004a, 2004b; Vršnak *et al.*, 2006). To resolve whether a particular shock was driven by a CME or ignited by a flare it is necessary to combine complete and detailed observations with theory. Such an analysis is presented herein, confronting the kinematics and evolution of the shock wave signatures with kinematics of the associated CME recorded on 24 December 1996. Results are compared with the theoretical model of the 3D piston scenario, which models the formation of large-scale disturbances in the solar corona (Žic *et al.*, 2008).

## 2. Description of the Event

### 2.1. The Data

Our analysis is based on the following set of observations:

- Dynamic spectra recorded by the spectrographs of the Astrophysical Institute Potsdam (AIP; Mann *et al.*, 1992), in the frequency range 40 – 800 MHz, and with a time resolution of 0.1 s
- Positions of the radio sources at 237, 164, and 151 MHz measured by the Nançay Radioheliograph (NRH; Kerdraon and Delouis, 1997), with a time resolution of 0.5 s
- GOES soft X-ray (SXR) flux measurements
- EUV observations of waves and early CME signatures provided by the Extreme-ultraviolet Imaging Telescope (EIT; Delaboudinière *et al.*, 1995), aboard the Solar and Heliospheric Observatory (SoHO), and
- Kinematics of the associated CME obtained using the LASCO-SOHO C1 and C2 data (Large Angle Spectroscopic Coronagraph; Brueckner *et al.*, 1995).

### 2.2. Characteristics of the Flare and Radio Event

The studied event is related to the GOES C2.1 flare from the active region NOAA 8007/8004 (N05° W74°/N06° W85°). The flare started at 13:05 UT and attained its maximum at about 13:11 UT (Figure 1c). The soft X-ray emission decreased to the background level in about 1.5 hours. The flare was preceded by the soft X-ray precursor at 12:30 – 13:05 UT.

In a large number of solar flares the time integral of the hard X-ray emission closely matches the rising part of the soft X-ray emission, what is known as the Neupert effect (Neupert, 1968; Veronig *et al.*, 2002; Brown and Kontar, 2005). The soft X-ray curve shows its steepest rise at 13:05:30 and a maximum at 13:11 UT. According to the Neupert effect, these times correspond to the maximum and end of the hard X-ray emission.

During the time interval 13:04:30 – 13:09:00 UT, radio observations in the microwave range (2.0 – 4.5 GHz) show intense type III-like bursts that indicate the impulsive phase of the associated flare. Between 13:09 and 13:26 UT, the AIP dynamic spectrum reveals distinct emission features of metric type II bursts, slowly drifting from 170 MHz toward lower frequencies (Figure 1a). Rather faint metric type III-like bursts, observed from 13:04 to 13:08 UT in the frequency range 40 – 400 MHz, preceded these metric type II bursts. Also a faint type II precursor[1] (Klassen *et al.*, 1999) is found at 13:04:30 – 13:11:30 UT, in the frequency range 200 – 400 MHz. In Figure 1a type III-like bursts and precursor are almost invisible owing to background subtraction, which was used to emphasize the more intense type II bursts. A strong type III burst was found in the DH/km range (10 000 – 200 kHz), starting from 13:05:30 UT and lasting about half an hour. Later on, a few type III bursts were recorded in the km range, at approximately 14:30, 16:00, and 19:00 UT; however, starting frequencies of these type III bursts could not be related to the interplanetary extrapolation of the CME propagation.

Herein, we concentrate on the metric type II burst (denoted as 1st type II in Figure 1b), representing a signature of the coronal shock wave. The harmonic emission band of the type II burst is better defined than its fundamental band, as usually in the metric range (Vršnak *et al.*, 2001). The dynamic spectrum reveals that the harmonic band of the type II burst was split into two lanes; that is, a type II band split is observed (Nelson and Melrose, 1985; Vršnak *et al.*, 2001, 2002; Vršnak, Magdalenić, and Zlobec, 2004). The type II emission bands drifted toward lower frequencies at the rate $\mathrm{d}f/\mathrm{d}t = 0.2$ MHz s$^{-1}$.

After the 1st type II burst, a faint 2nd type II-like burst was also recorded. The high-frequency part of the 2nd type II is homologous to the 1st type II harmonic band (Figure 2), indicating that this is probably also the harmonic emission. This conclusion is supported by the fact that no emission was recorded at the double frequency, and that in metric type II bursts harmonic emission is usually stronger than the fundamental (Vršnak *et al.*, 2001).

This similarity indicates that there was a second shock wave passing through the coronal plasma, having similar characteristics to the first shock wave. However, the low-frequency part of the 2nd type II burst was not well defined (Figure 1b). It has the appearance of a group of possibly shock-accelerated (SA) type III bursts (Bougeret *et al.*, 1998; Dulk *et al.*, 2000; Cane, Erickson, and Prestage, 2002) and it is not completely clear if this is a part of the 2nd type II or just a high-frequency part of the km-type III bursts observed in the *Wind*/Waves dynamic spectrum (Figure 1a).

[1] By the definition of Klassen *et al.* (1999), a precursor is a group of fast drifting bursts (pulsations, U bursts, J bursts, or reversed slope bursts) with a restricted bandwidth. The center frequency of the precursor group lies at the backward extrapolation through the type II lane.

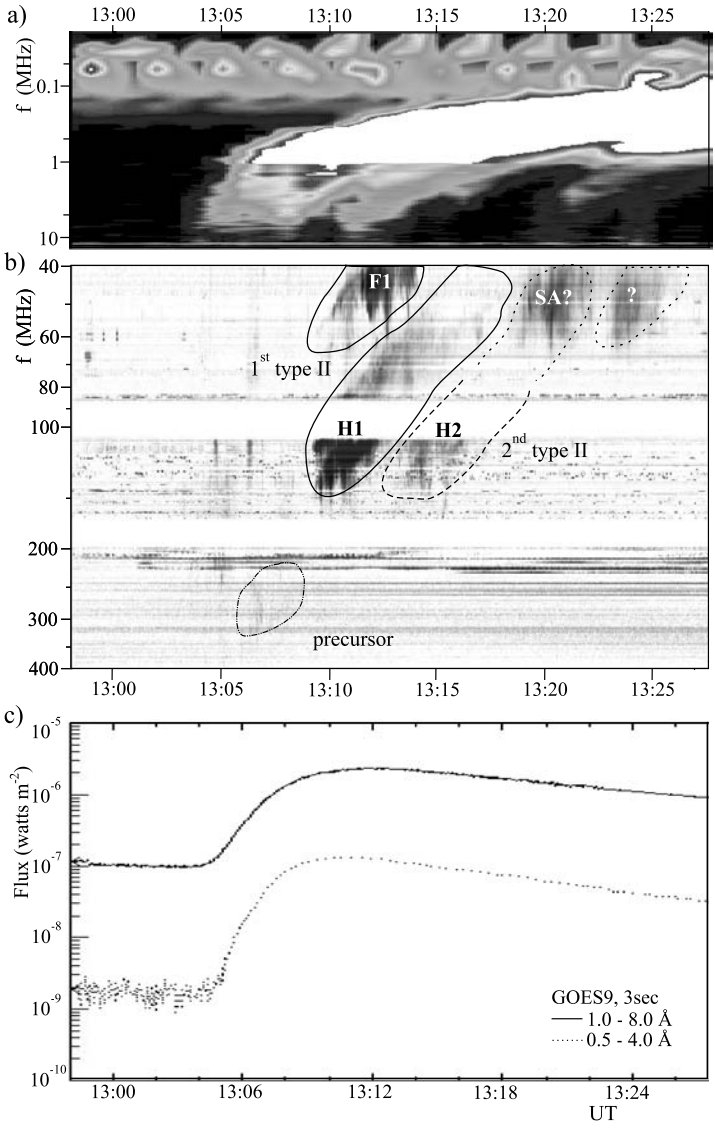


**Figure 1** (a) Dynamic spectrum recorded by WAVES (13.875 MHz – 20 kHz) on board the *Wind* spacecraft showing intense type III bursts of 24 December 1996. (b) Dynamic spectrum recorded by the AIP spectrographs, showing metric type II bursts and a faint type II precursor, recorded on 24 December 1996. Fundamental (F1) and harmonic (H1) emission band of the 1st type II are both well defined, whereas the second type II-like burst is rather patchy. SA denotes possibly shock-accelerated type III bursts. (c) GOES 1.0 – 8.0 and 0.5 – 4.0 Å fluxes, showing the temporal evolution of the flare soft X-ray emission.

## 2.3. Scaling of the Density Model and Type II Velocity

When interpreting frequency drifts of spectral radio features, the main problem is the choice of a proper density model. To demonstrate the ambiguity in the height estimate, we compared results obtained using two-fold and ten-fold Saito density models (2× and 10× Saito;

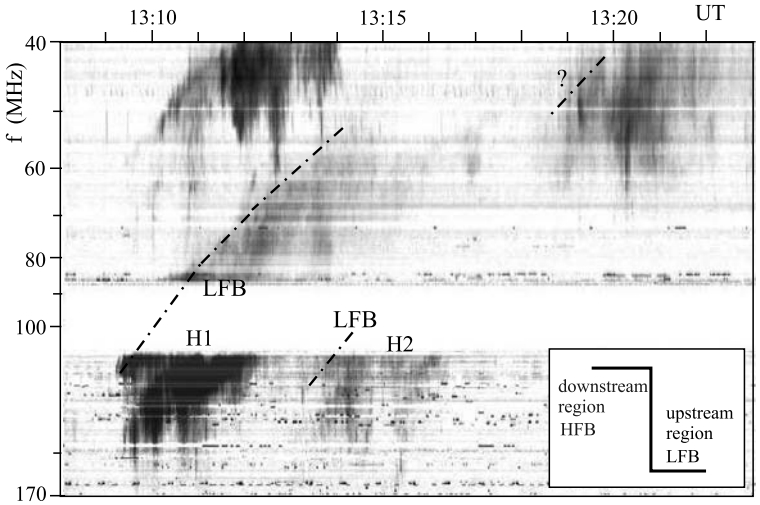


**Figure 2** Enlarged AIP dynamic spectrum showing bursty, spraylike structure of the type II bursts. The high-frequency parts of the harmonic band of the 1st and 2nd type II burst are homologous. In the inset a schematic drawing of the shock profile is shown; HFB and LFB denote high- and low-frequency components of the type II band split emitted from the downstream and the upstream regions.

Saito, 1970). The difference of the obtained heights found when using 2× and 10× Saito, can be as large as 0.5 solar radii (0.5 $R_\odot$). However, since the eruption took place close to the solar limb, where the influence of projection effects is expected to be rather small, it is possible to scale the density model by using the positions of radio sources (*i.e.*, NRH observations). The evolution of the dominant NRH source was compared with the corresponding radio features in the AIP dynamic spectrum. We were able to identify radio source only for the harmonic band of the 1st type II burst. The starting frequency of the harmonic band of the 2nd type II burst is slightly lower than the NRH observing frequency of 164 MHz, and for this event there were no NRH data available at 151 MHz. It is found that the position of the radio source at 164 MHz, which corresponds to the harmonic band of the 1st type II burst, was at $R = 1.4\,R_\odot$. To obtain the electron density $n_e$ corresponding to the frequency $f = 164/2 = 82$ MHz, we employed the relationship $f \sim 9n_e^{1/2}$, where $n_e$ is expressed in $\mathrm{cm}^{-3}$ and $f$ in kHz. Comparing the radial dependence of the plasma density behavior for different density models, we concluded that the 3.5× Saito is the most suitable density model in this event.

When the "proper" density model is obtained, the velocity of the shock wave can be found from the frequency drift of the type II bursts. The type II radio source is observed at rather low frequency of 164 MHz, and in this range the coronal scattering might affect the position estimates (for details see Gary *et al.*, 1984, and references therein). Therefore, the type II velocity was calculated not only for 3.5× Saito but also for 2× and 4× Saito, to obtain a range of possible values. We focus on the lower frequency branch (*i.e.,* the upstream region) of the harmonic band of the 1st type II burst. The obtained type II velocities are 970, 1100, and 1170 $\mathrm{km\,s}^{-1}$ for density models 2×, 3.5× and 4× Saito, *i.e.*, the type II velocity is around 1000 $\mathrm{km\,s}^{-1}$.

The AIP dynamic spectrum (Figure 2) shows a harmonic band of the 1st type II burst split into two lanes, separated by $f_H - f_L \approx 34$ MHz (where $f_L$ and $f_H$ are low- and high-frequency lanes of the split). This lane separation, at $f_L = 110$ MHz, gives us a relative band

split BDW $= (f_{\rm H} - f_{\rm L})/f_{\rm L} \approx 0.3$. If the band split is attributed to the plasma emission from the upstream/downstream shock region (Smerd, Sheridan, and Stewart, 1974, 1975; Vršnak *et al.*, 2001), the BDW is related to the density jump at the shock front as $X = ({\rm BDW} + 1)^2$ (Vršnak *et al.*, 2001), giving $X = 1.6$. If we assume perpendicular propagation of the shock, the Alfvén Mach number is related to $X$ as $M_{\rm A}^2 = [X(X + 5 + 5\beta)]/2(4 - X)$ (Priest, 1982), giving $M_{\rm A} = 1.5$. With a shock velocity of $v_{\rm s} \approx 1000$ km s$^{-1}$ we find an Alfvén velocity of $v_{\rm A} = v_{\rm s}/M_{\rm A} \approx 670$ km s$^{-1}$ (for details of the procedure we refer to Vršnak *et al.*, 2002; Vršnak, Magdalenić, and Zlobec, 2004).

### 2.4. General Description and Kinematics of the CME

The Fe XII 195 Å EIT observations in the EUV range were used to measure kinematics of the EIT wave and the first signatures of the CME. The CME was clearly observed in the EUV range at 13:14 UT. However, traces of a rising structure, probably the early CME signature, are already visible at 13:02 UT (Figure 3a). We measured the height of the leading edge at several position angles, depicted by dashed lines in Figure 3a. We used the most extreme values of obtained heights (*i.e.*, minimum height at 13:02 UT and maximum height at 13:14 UT) to obtain the largest possible velocity of the CME. The largest CME velocity during the impulsive phase of the flare is 235 km s$^{-1}$ (in Figure 7 denoted as CME-maximum). Using average heights (in Figure 7 denoted as CME-average), we find a mean CME velocity of 110 km s$^{-1}$.

The EIT wave was traced in three consecutive images (Figure 3b), and the average velocity of the wave was 250 km s$^{-1}$. The distance of the EIT wave was measured from the midpoint of the CME footpoints. Since the velocity of the EIT wave fits well with the CME velocity it can be concluded that, in this case, the EIT wave is a surface signature of the CME (Chen, Fang, and Shibata, 2005). Note that the EIT wave propagated southward, *i.e.*, in the opposite direction from the type II burst source. However, a dim and diffuse northward propagating brightening could be also noticed (Figure 3b). The wave propagation in this direction was probably impeded by the magnetic field of the streamer (Figure 4).

The CME appeared in the LASCO-C1 field of view at 13:20 UT (see http://solar.gmu.edu/research/cme_c1/) and in the LASCO-C2 field of view at 13:28 UT (Figure 4). In the C2 field of view two methods of measurement were applied to obtain the spread of possible values: *i*) Several measurements were made along the leading edge of the CME; *ii*) structures that can be tracked in consecutive images were selected and followed. Both types of measurements gave similar results. Values reported in the LASCO catalog (http://cdaw.gsfc.nasa.gov/cme_list/), corresponding to the "outermost" CME front propagation, roughly coincide with the lower limit of the values obtained herein. The CME velocities in the time intervals 13:14 – 13:20 UT, 13:20 – 13:28 UT, and 13:28 – 13:58 UT were 560, 1110, and 500 km s$^{-1}$, respectively.

### 2.5. The CME and the Radio Source

Limb events are of special importance in studying the origin of coronal shocks, since they reveal the plane-of-sky position of the type II burst source, relative to the CME. In Figure 5a, contours of the NRH radio source, corresponding to the harmonic band of the 1st type II burst, are superimposed on the EIT image with clearly visible leading edge of the CME. The first impression is that the shock wave is very close to the leading edge of the CME, or maybe even passing through the CME as in the case of 3 November 2003 (Vršnak *et al.*, 2006). However, a correction in time is needed since the EIT image is recorded at 13:14:14

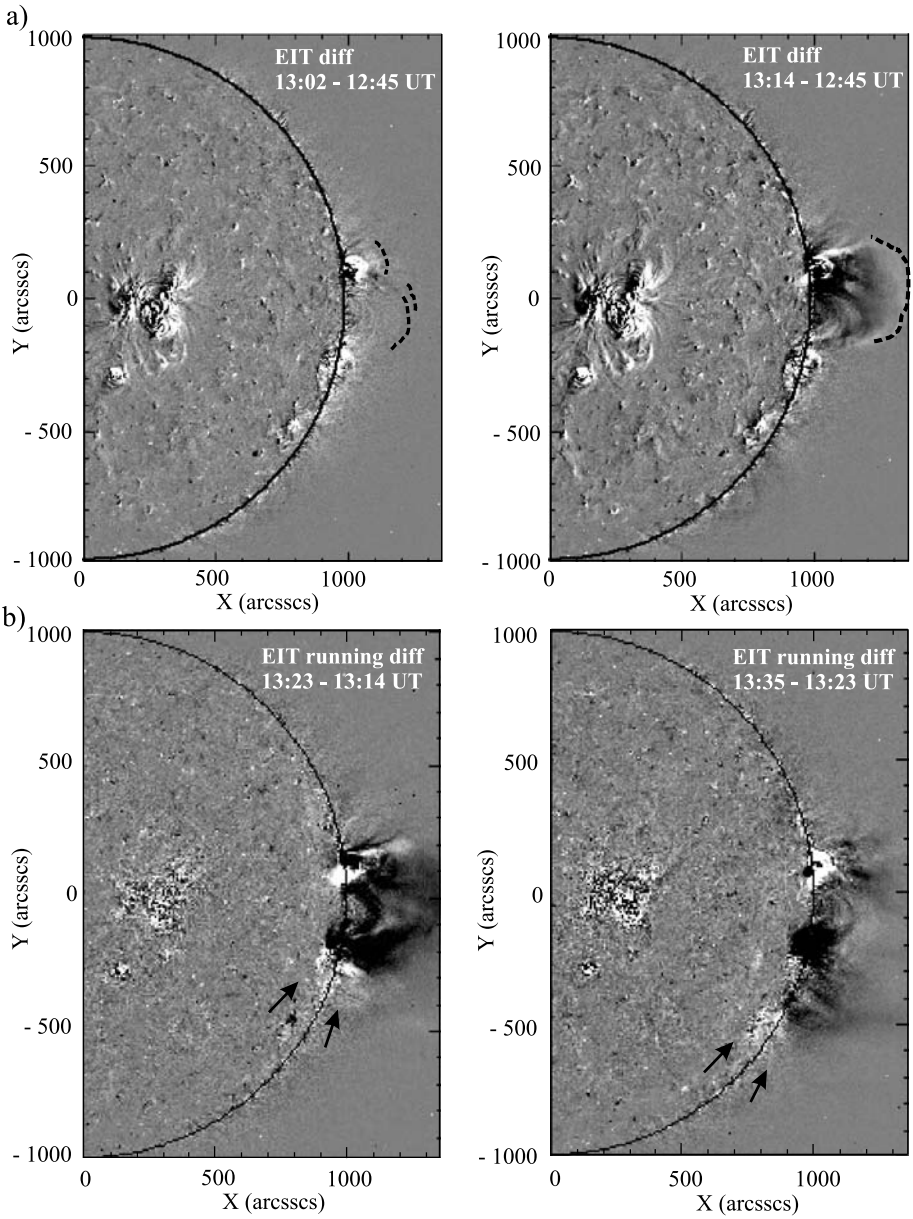


**Figure 3** (a) Leading edge of the CME shown in the base-difference EIT images (in which the pre-event image taken at 12:45 UT is subtracted from the other images), emphasized by dashed lines. (b) EIT running-difference images (in which the previous image of a sequence is subtracted from every image) showing signatures of the EIT wave. Arrows indicate the EIT wavefront.

UT and the NRH radio source at 13:10:07 UT. Taking into account the average velocity of the type II burst, $v_{\text{type II}} = 1000\ \text{km}\,\text{s}^{-1}$, and the time difference between two images, $\Delta t = 4.12$ minutes, we can calculate the distance encompassed by the shock wave. After

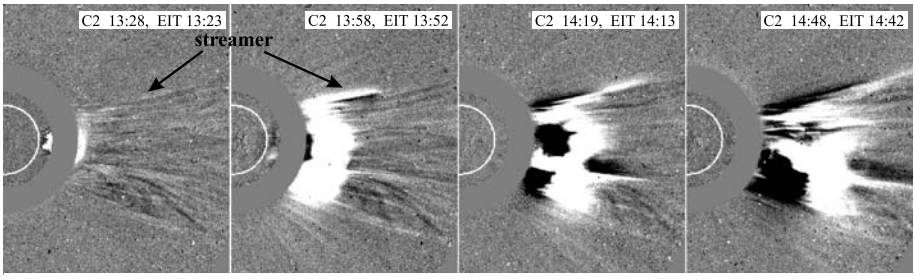


**Figure 4** The LASCO-C2 running-difference images combined with temporally closest EIT images showing propagation of the CME.

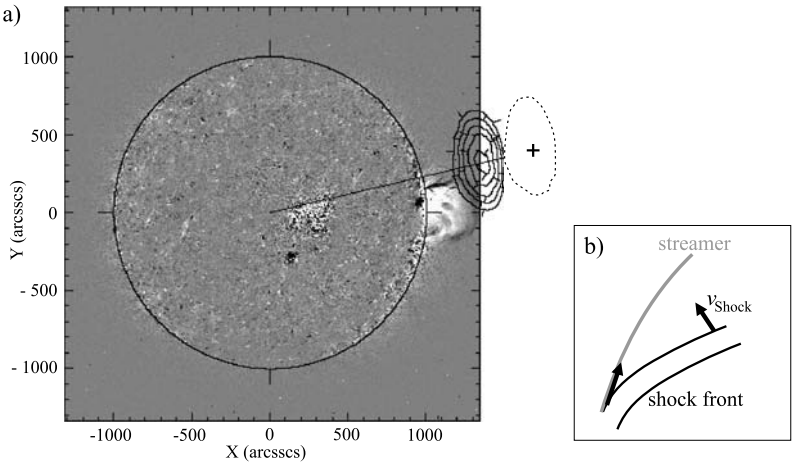


**Figure 5** (a) NRH radio source (13:10:07 UT), corresponding to the harmonic band of the 1st type II burst (H1), superposed on the EIT image (13:14:14 UT). The corrected position of the radio source is marked by the cross and dashed curve. (b) Geometry of the shock front and the field line of the streamer; such an interaction between the shock front and the streamer can lead to a significant overestimate of the radio source velocity.

this correction the distance between radio source and shock wave is in the range of 300 – 356 Mm, depending on which part of the CME leading edge is considered. In Figure 5a the new position of the radio source is depicted by the cross and dashed curve.

## 3. Discussion and Conclusions

We presented a multiwavelength study of the CME – flare event recorded on 24 December 1996, focusing on the wave – CME/flare relationship. Figures 6 and 7 show the kinematics of the shock wave signatures compared with the CME kinematics.

In Figure 6 the time interval 13:00 – 15:00 UT is considered, showing all measurements in the LASCO-C2 field of view. In this event, flare and CME are not synchronized (Figure 6); that is, the flare impulsive phase (marked by the black triangle) and acceleration of the CME (gray triangle) do not coincide in time. The maximum and the end of the impulsive phase of the flare were at 13:04:30 UT and 13:11:02 UT, respectively. The CME acceleration peaked

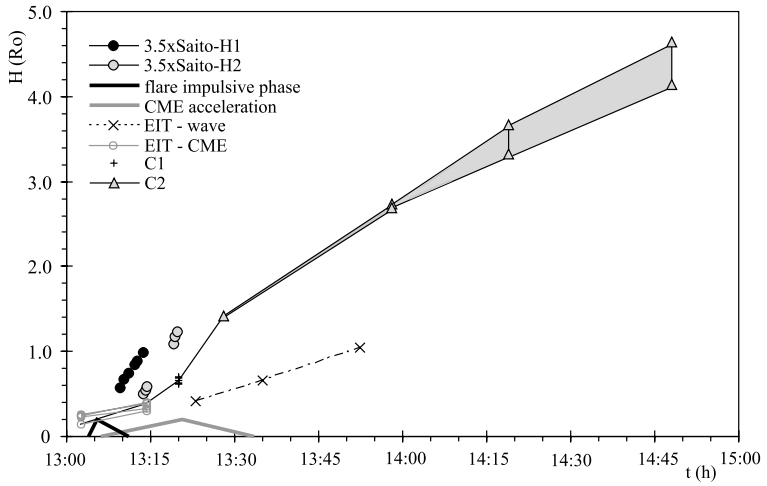


**Figure 6** Kinematics of the CME compared with signatures of the shock wave and EIT wave. Note that the EIT wave propagates in the horizontal direction. The *y*-axis represents the height above the photosphere. The positions of the 1st and 2nd type II burst sources (H1 and H2) are denoted by black and gray dots, respectively. The shaded area represents a span of heights measured at several position angles along the leading edge of the CME.

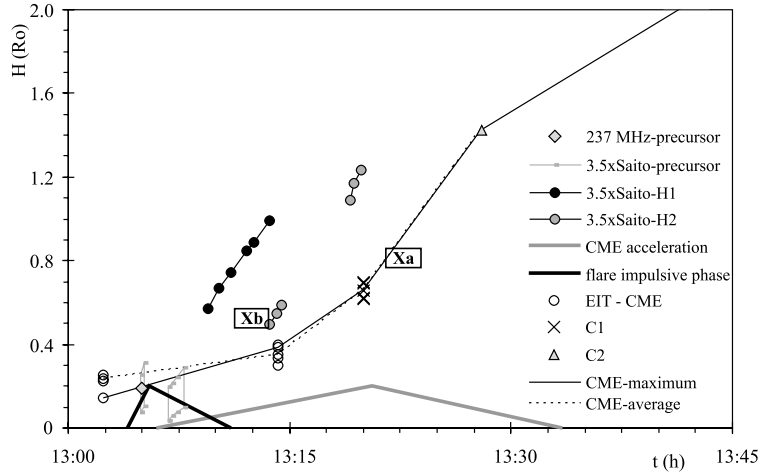


**Figure 7** Kinematics of the CME and shock wave signatures, focused on the acceleration phase of the CME. The height above the photosphere is shown as a function of time.

about 10 min after the end of the impulsive phase of the flare (*i.e.*, at 13:20:33 UT), and acceleration ended around 13:33:28 UT (Figures 6 and 7).

In the interval of interest, 13:02 – 13:30 UT, both the "mean" and the highest possible velocity of the CME (110 and 235 km s$^{-1}$, respectively) are comparable with the velocity of the EIT wave, 250 km s$^{-1}$ (Figures 6). Since the back-extrapolation from the EIT wave marks the beginning of the CME rise as well, we conclude that in this case, the EIT wave

was probably a low coronal signature of the field line "opening" caused by the CME (Chen, Fang, and Shibata, 2005).

Figure 7 shows the shock wave and CME kinematics, focusing on the acceleration phase of the CME and the impulsive phase of the flare. The back-extrapolation of the type II burst fits well with the flare impulsive phase, indicating that the shock wave could be generated by the explosive energy release in the flare.

The kinematical curves of both the 1st type II burst and the 2nd type II-like burst were ahead of the kinematical curve of the CME (Figure 6). Moreover, as shown in Figure 7, the CME acceleration reaches maximum after the type II emission. The velocity of the type II burst was about 1000 km s$^{-1}$ and the velocity of the CME, at the time of type II burst appearance was at most 235 km s$^{-1}$, and on average around 110 km s$^{-1}$. We stress that the shock velocity was almost an order of magnitude larger than the CME velocity. Moreover, in estimating the shock velocity we assumed radial propagation of the radio source. If the trajectory was inclined the obtained velocity is underestimated and the difference between the shock and CME velocities was even larger.

Since the velocity of the CME was subsonic, we can exclude the bow shock scenario as a mechanism of shock formation. Moreover, in the bow shock scenario the shock and driver propagate at comparable speeds, which is not the case in this event.

Since the bow shock scenario is excluded, we employ the 3D piston scenario (Žic *et al.*, 2008). In this model a spherical expansion of the driver is analyzed. We consider two possibilities: *i*) The CME accelerates from 0 to 250 km s$^{-1}$, which gives an average velocity $v_{\rm av} = 125$ km s$^{-1}$; *ii*) the CME accelerates from 0 to 500 km s$^{-1}$, which gives an average velocity $v_{\rm av} = 250$ km s$^{-1}$.

These two possibilities were used because average velocities are approximately equal to the "mean" and highest possible CME velocity (110 and 235 km s$^{-1}$, respectively) in the interval of interest. It was found that only in the second case, and with an ambient Alfvén velocity $\leq$400 km s$^{-1}$, can the CME be considered as a possible driver of the 2nd shock wave. Namely, employing the results presented by Žic *et al.* (2008), we find that, with the average CME velocity of 250 km s$^{-1}$, the shock wave would form in 10 minutes. During this time the CME would pass about 150 Mm, and the shock would occur at a distance of roughly 350 Mm. We considered that acceleration starts at the moment of first observation of the CME. In Figure 7 the position of the shock formation (marked by the symbol "Xb") with respect to the CME kinematical curve is shown. The shock formation point Xb is not far from the 2nd shock wave; however, it is slightly higher than the shock and it is not certain that the CME could drive this shock.

In the case of an average CME velocity of 125 km s$^{-1}$, the CME cannot be considered as a driver of the shock, even if we assume an ambient Alfvén velocity $\leq$400 km s$^{-1}$. In this case, according to Žic *et al.* (2008), the shock would form in about 20 minutes at a distance of 550 Mm. The point of shock formation for this case is marked in Figure 7 by "Xa." It is very clear that under such circumstances the CME cannot be considered as a driver of the shock wave.

Let us stress that in both considered options a rather low Alfvén velocity was assumed and that the shock velocity is almost an order of magnitude larger than the CME velocity. The considered ambient Alfvén velocity is almost half the value of the Alfvén velocity obtained from the band split, $v_{\rm A} = 700$ km s$^{-1}$. If the model would consider a higher Alfvén velocity, and the same average CME velocities, the time needed for the shock formation would be considerably longer, and in that case the CME as a driver of the shock wave can be completely excluded.

We also examined the possibility that the shock velocity obtained from the radio observations is overestimated. If we assume that the radio emission is excited at the nearby

streamer (Figures 4 and 5), analogous to the work of Mancuso and Raymond (2004), then the geometrical configuration is as shown in Figure 5b. In such a configuration, when the angle between the shock front and the field lines of the streamer is small, the apparent speed of the radio source could be very high. In this situation the velocity obtained from the drift of the type II burst can be largely overestimated. However, from Figures 4 and 5a we see that the shock wave propagates almost perpendicular to the streamer, so we conclude that in this event the shock velocity is most probably not overestimated.

An interesting aspect of the presented radio observations is also the homology of the two type II bursts. It should be noted that, regardless of the nature of the shock driver, the shock propagation is strongly affected by the spatial distribution of the coronal Alfvén velocity (*i.e.*, the shock preferably propagates along valleys of low Alfvén velocity; Uchida, 1974). Furthermore, radio emission from the shock is generally not observed along the whole shock front, but only from shock front segments favorable for the excitation of radio emission. The homology of the two observed type II bursts indicates that both shocks were propagating through plasmas having similar characteristics. Bearing in mind the time difference between the two type II bursts, we deduce that the corona needed less than 5 minutes to relax after the passage of the first shock. Such a conclusion is consistent with the Moreton wave observations, which show a relaxation time of a few minutes (Warmuth *et al.*, 2004b).

Taking into account all considerations and the theoretical approach of the 3D piston scenario, we can conclude that in this case it is not probable that the CME was a driver of the observed shock waves. Even if we consider the "best" possible scenario for the CME as a driver of the shock, the CME can be a driver only of the 2nd shock. Thus, our results show that in this event the first shock was not generated by the CME, but rather by a relatively weak flare (C2.1). This contrasts with the result of Cliver *et al.* (2004) that all coronal shocks are CME driven. The presence of the CME does not imply that the shock was launched and driven by the CME; however, we do not exclude the possibility that the presence of a CME might be a necessary condition for shock formation (Vršnak *et al.*, 2006).

**Acknowledgements** We are grateful to the referees whose critical comments and useful suggestions helped us to improve the paper. Furthermore, we are grateful to the staff of the Solar Radio Observatory of the Astrophysical Institute Potsdam and Nançay Radio Observatory, as well as to the *Wind*/WAVES and SOHO teams for their open data policy. J.M. and B.V. acknowledge funding by the Croatian Ministry of Science, Education and Sports under Project No. 007-0000000-1362. M.T. acknowledges funding by the Austrian Fonds zur Förderung der wissenschaftlichen Forschung under Project Nos. P20145-N16 and J2512-N02. S.P. and N.J.L. acknowledge partial support from the Academy of Finland Project No. 104329.

## References

Biesecker, D.A., Myers, D.C., Thompson, B.J., Hammer, D.M., Vourlidas, A.: 2002, Solar phenomena associated with "EIT waves". *Astrophys. J.* **569**, 1009 – 1015. doi:10.1086/339402.

Bougeret, J.L., Zarka, P., Caroubalos, C., Karlický, M., Leblanc, Y., Maroulis, D., Hillaris, A., Moussas, X., Alissandrakis, C.E., Dumas, G., Perche, C.: 1998, A shock associated (SA) radio event and related phenomena observed from the base of the solar corona to 1 AU. *Geophys. Res. Lett.* **25**, 2513 – 2516. doi:10.1029/98GL50563.

Brown, J.C., Kontar, E.P.: 2005, Problems and progress in flare fast particle diagnostics. *Adv. Space Res.* **35**, 1675 – 1682. doi:10.1016/j.asr.2005.03.020.

Brueckner, G.E., Howard, R.A., Koomen, M.J., Korendyke, C.M., Michels, D.J., Moses, J.D. *et al.*: 1995, The large angle spectroscopic coronagraph (LASCO). *Solar Phys.* **162**, 357 – 402. doi:10.1007/BF00733434.

Cane, H.V., Erickson, W.C., Prestage, N.P.: 2002, Solar flares, type III radio bursts, coronal mass ejections, and energetic particles. *J. Geophys. Res. (Space Phys.)* **107**, 1315 – 1333. doi:10.1029/2001JA000320.

Chen, P.F., Fang, C., Shibata, K.: 2005, A full view of EIT waves. *Astrophys. J.* **622**, 1202 – 1210. doi:10.1086/428084.

Cliver, E.W., Webb, D.F., Howard, R.A.: 1999, On the origin of solar metric type II bursts. *Solar Phys.* **187**, 89 – 114.
Cliver, E.W., Nitta, N.V., Thompson, B.J., Zhang, J.: 2004, Coronal shocks of November 1997 revisited: The CME type II timing problem. *Solar Phys.* **225**, 105 – 139. doi:10.1007/s11207-004-3258-1.
Delaboudinière, J.P., Artzner, G.E., Brunaud, J., Gabriel, A.H., Hochedez, J.F., Millier, F., *et al.*: 1995, EIT: extreme-ultraviolet imaging telescope for the SOHO mission. *Solar Phys.* **162**, 291 – 312. doi:10.1007/BF00733432.
Dulk, G.A., Leblanc, Y., Bastian, T.S., Bougeret, J.L.: 2000, Acceleration of electrons at type II shock fronts and production of shock-accelerated type III bursts. *J. Geophys. Res.* **105**, 27343 – 27352. doi:10.1029/2000JA000076.
Gary, D.E., Dulk, G.A., House, L., Illing, R., Sawyer, C., Wagner, W.J., McLean, D.J., Hildner, E.: 1984, Type II bursts, shock waves, and coronal transients – The event of 1980 June 29, 0233 UT. *Astron. Astrophys.* **134**, 222 – 233.
Hudson, H.S., Khan, J.I., Lemen, J.R., Nitta, N.V., Uchida, Y.: 2003, Soft X-ray observation of a large-scale coronal wave and its exciter. *Solar Phys.* **212**, 121 – 149. doi:10.1023/A:1022904125479.
Kerdraon, A., Delouis, J.M.: 1997, The Nançay radioheliograph. In: Trottet, G. (ed.) *Coronal Physics from Radio and Space Observations*, *Lecture Notes in Physics* **483**, Springer, Berlin, 192 – 201.
Klassen, A., Aurass, H., Klein, K.L., Hofmann, A., Mann, G.: 1999, Radio evidence on shock wave formation in the solar corona. *Astron. Astrophys.* **343**, 287 – 296.
Mancuso, S., Raymond, J.C.: 2004, Coronal transients and metric type II radio bursts. I. Effects of geometry. *Astron. Astrophys.* **413**, 363 – 371. doi:10.1051/0004-6361:20031510.
Mann, G., Aurass, H., Voigt, W., Paschke, J.: 1992, Preliminary observations of solar type 2 bursts with the new radiospectrograph in Tremsdorf (Germany). In: Mattok, C. (ed.) *Coronal Streamers, Coronal Loops, and Coronal and Solar Wind Composition*, *SP* **348**, ESA, Noordwijk, 129 – 132.
McLean, D.J., Labrum, N.R.: 1985, *Solar Radiophysics: Studies of Emission from the Sun at Meter Wavelengths*, Cambridge University Press, Cambridge.
Moreton, G.E., Ramsey, H.E.: 1960, Recent observations of dynamical phenomena associated with solar flares. *Pub. Astron. Soc. Pac.* **72**, 357 – 358.
Nelson, G.J., Melrose, D.B.: 1985, Type II bursts. In: McLean, D.J., Labrum, N.R. (eds.) *Solar Radiophysics: Studies of Emission from the Sun at Metre Wavelengths*, Cambridge University Press, Cambridge, 333 – 359.
Neupert, W.M.: 1968, Comparison of solar X-ray line emission with microwave emission during flares. *Astrophys. J.* **153**, L59 – L64.
Oh, S.Y., Yi, Y., Kim, Y.H.: 2007, Solar cycle variation of the interplanetary forward shock drivers observed at 1 AU. *Solar Phys.* **245**, 391 – 410.
Priest, E.R.: 1982, *Solar Magnetohydrodynamics*, D. Reidel, Dordrecht.
Reiner, M.J., Kaiser, M.L., Gopalswamy, N., Aurass, H., Mann, G., Vourlidas, A., Maksimovic, M.: 2001, Statistical analysis of coronal shock dynamics implied by radio and white-light observations. *J. Geophys. Res.* **106**, 25279 – 25290. doi:10.1029/2000JA004024.
Saito, K.: 1970, A non-spherical axisymmetric model of the solar K corona of the minimum type. *Ann. Tokyo Astron. Obs.* **12**, 53 – 137.
Smerd, S.F., Sheridan, K.V., Stewart, R.T.: 1974, On split-band structure in type II radio bursts from the Sun. In: Newkirk, G.A. (ed.) *Coronal Disturbances*, *IAU Symp.* **57**, 389 – 393.
Smerd, S.F., Sheridan, K.V., Stewart, R.T.: 1975, Split-band structure in type II radio bursts from the Sun. *Astrophys. Lett.* **16**, 23 – 28.
Uchida, Y.: 1968, Propagation of hydromagnetic disturbances in the solar corona and Moreton's wave phenomenon. *Solar Phys.* **4**, 30 – 44. doi:10.1007/BF00146996.
Uchida, Y.: 1974, Behavior of the flare produced coronal MHD wavefront and the occurrence of type II radio bursts. *Solar Phys.* **39**, 431 – 449.
Veronig, A., Vršnak, B., Dennis, B.R., Temmer, M., Hanslmeier, A., Magdalenić, J.: 2002, Investigation of the Neupert effect in solar flares. I. Statistical properties and the evaporation model. *Astron. Astrophys.* **392**, 699 – 712. doi:10.1051/0004-6361:20020947.
Vršnak, B.: 2001, Solar flares and coronal shock waves. *J. Geophys. Res.* **106**, 25291 – 25300. doi:10.1029/2000JA004009.
Vršnak, B., Magdalenić, J., Zlobec, P.: 2004, Band-splitting of coronal and interplanetary type II bursts. III. Physical conditions in the upper corona and interplanetary space. *Astron. Astrophys.* **413**, 753 – 763. doi:10.1051/0004-6361:20034060.
Vršnak, B., Aurass, H., Magdalenić, J., Gopalswamy, N.: 2001, Band-splitting of coronal and interplanetary type II bursts. I. Basic properties. *Astron. Astrophys.* **377**, 321 – 329. doi:10.1051/0004-6361:20011067.
Vršnak, B., Magdalenić, J., Aurass, H., Mann, G.: 2002, Band-splitting of coronal and interplanetary type II bursts. II. Coronal magnetic field and Alfvén velocity. *Astron. Astrophys.* **396**, 673 – 682. doi:10.1051/0004-6361:20021413.

Vršnak, B., Warmuth, A., Temmer, M., Veronig, A., Magdalenić, J., Hillaris, A., Karlický, M.: 2006, Multi-wavelength study of coronal waves associated with the CME-flare event of 3 November 2003. *Astron. Astrophys.* **448**, 739 – 752. doi:10.1051/0004-6361:20053740.

Warmuth, A., Vršnak, B., Magdalenić, J., Hanslmeier, A., Otruba, W.: 2004a, A multiwavelength study of solar flare waves. I. Observations and basic properties. *Astron. Astrophys.* **418**, 1101 – 1115. doi:10.1051/0004-6361:20034332.

Warmuth, A., Vršnak, B., Magdalenić, J., Hanslmeier, A., Otruba, W.: 2004b, A multiwavelength study of solar flare waves. II. Perturbation characteristics and physical interpretation. *Astron. Astrophys.* **418**, 1117 – 1129. doi:10.1051/0004-6361:20034333.

Žic, T., Vršnak, B., Temmer, M., Jacobs, C.: 2008, Cylindrical and spherical pistons as drivers of MHD shocks. *Solar Phys.*, in press. doi:10.1007/s11207-008-9173-0.